

UNCLASSIFIED

Defense Technical Information Center  
Compilation Part Notice

ADP011867

TITLE: Crystal Growth of New Functional Materials for Electro-Optical Applications

DISTRIBUTION: Approved for public release, distribution unlimited

This paper is part of the following report:

TITLE: International Conference on Solid State Crystals 2000: Growth, Characterization, and Applications of Single Crystals Held in Zakopane, Poland on 9-12 October 2000

To order the complete compilation report, use: ADA399287

The component part is provided here to allow users access to individually authored sections of proceedings, annals, symposia, etc. However, the component should be considered within the context of the overall compilation report and not as a stand-alone technical report.

The following component part numbers comprise the compilation report:

ADP011865 thru ADP011937

UNCLASSIFIED

# Crystal growth of new functional materials for electro-optical applications

T.Fukuda\*, K.Shimamura, A.Yoshikawa and E.G.Villora

Institute for Materials Research, Tohoku University, Sendai 980-8577, Japan

## ABSTRACT

High quality fluoride and oxide single crystals for optical, piezoelectric and other applications have been grown by advanced crystal growth techniques. Corquitiite- and Perovskite-type fluoride single crystals –  $\text{LiCaAlF}_6$ ,  $\text{LiSrAlF}_6$ ,  $\text{KMgF}_3$  and  $\text{BaLiF}_3$  – have been grown for solid state UV laser applications, and as window materials for next generation optical lithography.  $\text{La}_3\text{Nb}_{0.5}\text{Ga}_{5.5}\text{O}_{14}$  and  $\text{La}_3\text{Ta}_{0.5}\text{Ga}_{5.5}\text{O}_{14}$  piezoelectric single crystals of size and quality comparable to  $\text{La}_3\text{Ga}_5\text{SiO}_{14}$  (langasite), have been produced. The piezoelectric and device properties of the crystals were investigated. A search for new langasite-type materials was also performed. Promising new structural materials,  $\text{Al}_2\text{O}_3/\text{RE}_3\text{Al}_5\text{O}_{12}$  (RE=rare earth) eutectic fibers, have been grown by the micro-pulling-down ( $\mu$ -PD) technique. Undoped and doped  $\beta$ - $\text{Ga}_2\text{O}_3$  single crystals have been grown by the floating zone technique as promising transparent conductive oxides.

## 1. INTRODUCTION

The important role of oxide and fluoride crystals in various branches of science and technology demands a comprehensive and integrated treatment of the subject. We have carried out investigations focusing on the development of new materials for optical, piezoelectric and other applications, using advanced crystal growth techniques. Oxide crystals are of highest importance for modern electrical and electro-optical applications in several devices. Fluoride single crystals, because of their unique properties such as large band gap, also present many advantages as optical materials.

The recent crystal growth research described in this work involved the development of new, high-quality oxide and fluoride single crystals, and of novel crystal growth techniques. The growth of fluoride single crystals doped with Ce for ultra-violet (UV) laser applications is reviewed. Growth of new langasite ( $\text{La}_3\text{Ga}_5\text{SiO}_{14}$ ) single crystals for piezoelectric applications, by the Czochralski (CZ) technique, is discussed. The micro-pulling-down ( $\mu$ -PD) method and its application to the growth of structural materials are mentioned. Crystal growth of  $\beta$ - $\text{Ga}_2\text{O}_3$  for transparent conductive oxide (TCO) applications is also addressed.

## 2. FLUORIDES FOR UV OPTICAL APPLICATIONS

Coherent optical sources in the ultraviolet (UV) wavelength region are useful for many practical applications, such as medical procedures, semiconductor processing and remote sensing<sup>1</sup>. Recently, Ce-doped  $\text{LiCaAlF}_6$  (Ce:LiCAF) and  $\text{LiSrAlF}_6$  (Ce:LiSAF) single crystals have been reported as leading candidates for tunable all-solid-state-lasers in the UV wavelength region<sup>2,3</sup>. However, due to the limited size of the available crystals, it was difficult to obtain high energy output directly from a Ce:LiCAF laser. Furthermore, the growth of Ce:LiCAF itself was known to be difficult<sup>4</sup>.

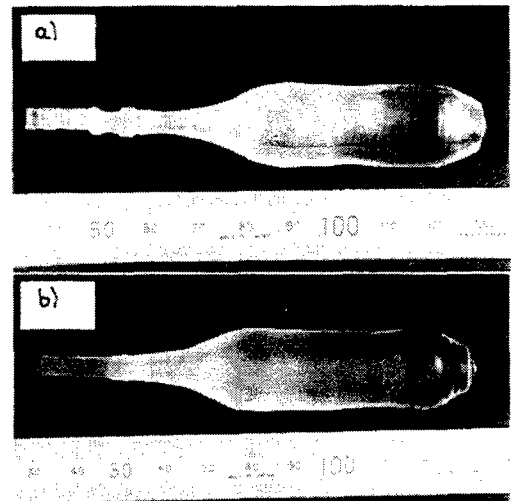


Fig.1 As-grown Ce-doped (a)  $\text{LiCaAlF}_6$  and (b)  $\text{LiSrAlF}_6$  single crystals.

\* T.F.: Email: fukuda@lexus.imr.tohoku.ac.jp; Telephone: +81-22-215-2100; Fax: +81-22-215-2101  
 K.S.: Email: shimak@lexus.imr.tohoku.ac.jp; Telephone: +81-22-215-2103; Fax: +81-22-215-2104  
 A.Y.: Email: yoshikaw@lexus.imr.tohoku.ac.jp  
 E.G.V.: Email: villora@lexus.imr.tohoku.ac.jp

Crystal growth was performed in a CZ system with a resistive heater made of high-purity graphite. The starting material was prepared from commercially available  $\text{AlF}_3$ ,  $\text{CaF}_2$ ,  $\text{SrF}_2$ , and  $\text{LiF}$  powders of high purity (>99.99%). The composition was 1 mol.%  $\text{LiF}$  and  $\text{AlF}_3$  enriched from a stoichiometric one, in order to compensate for the vaporization of  $\text{LiF}$  and  $\text{AlF}_3$ . As dopants,  $\text{CeF}_3$  and  $\text{NaF}$  powders of high purity (>99.99%, Rare Metallic Co., Ltd.) were used.  $\text{Na}^+$  was co-doped with  $\text{Ce}^{3+}$  in order to maintain the charge neutrality. The concentration of  $\text{Ce}^{3+}$  and  $\text{Na}^+$  in the starting material was 1 mol.%. The pulling rate was 1 mm/h and the rotation rate was 10 rpm. Crystal growth was performed under high purity  $\text{CF}_4$  gas (99.9999%).

Fig.1 shows as-grown Ce:LiCAF and Ce:LiSAF single crystals with dimensions of 18 mm in diameter and 60 mm in length. Cracks, bubbles and inclusions were not observed. Under the modified growth conditions, foreign substances on the surface of the grown crystal, as observed in ref.5, were not formed. However, Ce:LiSAF showed a tendency to crack perpendicular to the growth axis after several days. On the contrary, Ce:LiCAF did not show cracks at any time. Therefore, LiCAF was chosen for the growth of large diameter crystals. The effective distribution coefficient ( $k_{\text{eff}}$ ) of  $\text{Ce}^{3+}$  in LiCAF and LiSAF has been determined to be 0.021 and 0.013, respectively. The  $k_{\text{eff}}$  of  $\text{Ce}^{3+}$  in LiCAF was larger than in LiSAF. This is because the ionic radius of  $\text{Ce}^{3+}$  under 6-fold coordination (1.01 Å) is closer to that of  $\text{Ca}^{2+}$  (1.00 Å) than to that of  $\text{Sr}^{2+}$  (1.18 Å)<sup>6</sup>, the ions thought to be replaced by  $\text{Ce}^{3+}$ <sup>5</sup>.

Fig.2 shows an as-grown Ce:LiCAF single crystal of 2-inch diameter, free from cracks and inclusions. When crystals of this diameter were grown, the following two problems, not observed for crystals of 18 mm diameter, appeared: formation of inclusions, and cracks accompanied by the formation of an impurity phase at the bottom of the crystal.

Fig.3 shows a crystal which contains inclusions. It should be noticed that the formation of these inclusions was related to a change of the crystal diameter, for example at the shoulder part of the crystal. Once they appeared at the shoulder part, they did not disappear during crystal growth. In order to avoid these inclusions, the diameter at the shoulder part had to be controlled precisely and extended smoothly, without rapid change of the diameter. Although the absorption spectrum for the inclusion free region did not show any absorption peaks, that of the region with inclusions had one small absorption peak around  $3600\text{ cm}^{-1}$ . Since this peak indicates the existence of  $\text{OH}^-$ , it is thought that  $\text{H}_2\text{O}$  based impurities were present in the inclusions.

Fig.4 shows an as-grown crystal with one large crack along the growth axis and a white substance at the bottom of the crystal. This large, flat crack appeared during cooling after growth, in cases when white material was present. This white substance usually formed when the solidification fraction exceeded 70%. The XRD analysis showed that the white substance was composed of LiCAF and  $\text{CaF}_2$  phases. This is because the melt composition shifted in the  $\text{CaF}_2$ -enriched direction during growth, since the vaporization pressure of  $\text{LiF}$  and  $\text{AlF}_3$  is very high<sup>7</sup>.  $\text{CeF}_3$  and  $\text{NaF}$  might have accumulated in the residual melt due to the small  $k_{\text{eff}}$ . In order to avoid formation of this white substance, crystal growth was terminated at the solidification fraction 60%, as for the crystal shown in Fig.2. For further improvement, optimization of melt composition should be carried out.

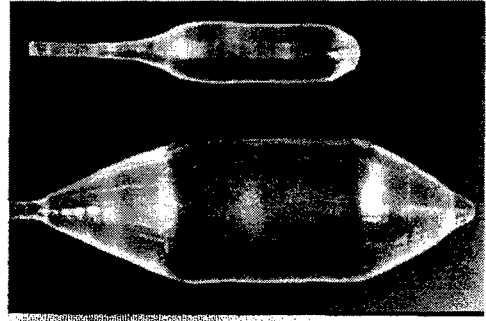


Fig.2 2 inch size Ce,Na:LiCaAlF<sub>6</sub> single crystal. compared with 1 inch crystal.

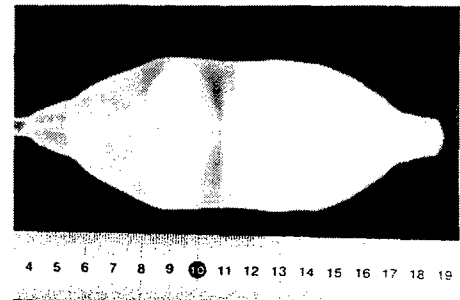


Fig.3 Ce:LiCaAlF<sub>6</sub> crystal with inclusions.

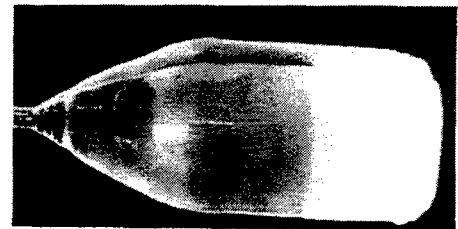


Fig.4 Ce:LiCaAlF<sub>6</sub> crystal with white substances.

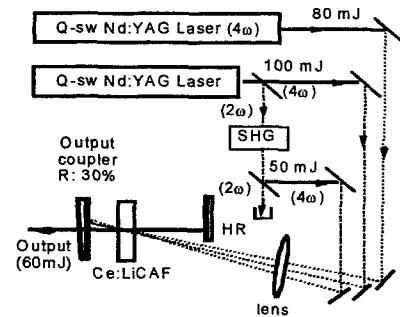


Fig.5 Ce:LiCaAlF<sub>6</sub> laser setup.

We have already demonstrated an output energy of 30 mJ from a UV solid-state Ce:LiCAF laser that operated at 290 nm at a repetition rate of 10 Hz<sup>5,8</sup>. In order to obtain higher output energy, we increased the pumping energy. Fig.5 shows a setup for laser experiments. We obtained 60 mJ at 10 Hz, to our knowledge the highest performance so far reported for Ce:LiCAF.

Fig.6 shows the transmission edge of the LiCAF and LiSAF single crystals grown under Ar and CF<sub>4</sub> atmosphere. The transmission edge of LiCAF was measured to be at 112 nm and that of LiSAF 116 nm, the shortest reported to our knowledge. The absorption at around 125 nm observed from the crystals grown under Ar atmosphere, disappeared when crystals were grown under CF<sub>4</sub> atmosphere. These transmission characteristics of LiCAF and LiSAF show their high potential as optical window materials in the UV and VUV wavelength region.

Recently, there has been significant interest in using 157-nm laser sources in projection lithography as successors to 193-nm based system. One of the most serious problems in realizing a 157-nm based system is the development of suitable optical materials for lenses and other optical components. In particular, for an all-refractive design of 157-nm laser source, a second material other than CaF<sub>2</sub> is strongly required, because CaF<sub>2</sub> is the most promising material to be used. Primary candidates for a second material were LiF and MgF<sub>2</sub>; however, they have several disadvantages such as a fragile and hygroscopic nature and large birefringence<sup>9</sup>.

We have identified KMgF<sub>3</sub> (KMF) as a new promising optical material for 157-nm based system. The reasons to focus on KMF are as follows: (1) It belongs to the cubic crystal system<sup>10</sup>, so theoretically it has no birefringence. (2) As it is composed of K and Mg cations, which have smaller atomic weight than Ca, it can be expected to have a shorter transmission edge than CaF<sub>2</sub>. (3) As it melts congruently at a melting temperature of 1070 °C<sup>11</sup>, it can more likely be grown to a large size. BaLiF<sub>3</sub> (BLF) can also be a promising candidate, since it belongs to the cubic crystal system<sup>12</sup> and it can transmit 157-nm.

Crystal growth was performed in the same CZ system as for LiCAF and LiSAF. The starting material was prepared from commercially available high purity powders (>99.99%). The pulling rate was 0.5 to 1.5 mm/h and the rotation rate was 15 rpm.

Fig.7 shows an as-grown KMF and BLF single crystals 20 mm in diameter and 90 mm in length, pulled at a rate of 1 mm/h. No cracks, bubbles or inclusions were observed. The thermal expansion coefficients of KMF and BLF along <111> was estimated to be  $1.98 \times 10^{-5} \text{ K}^{-1}$  and  $3.06 \times 10^{-5} \text{ K}^{-1}$ , respectively, over the range 100 - 500 °C. The variations of birefringence among KMF-wafer, BLF-wafer and LiCAF-wafer were of order  $10^{-7}$ ,  $10^{-5}$ , and  $10^{-7}$ , respectively. Furthermore, the transmission edge of KMF and BLF single crystals was determined to be 115 nm and 120 nm. Fig.6 shows the transmission spectrum of KMF and BLF single crystals in VUV wavelength region, compared with LiCAF and LiSAF. These transmission characteristic of KMF and BLF single crystals shows its high potential as optical material in the UV and VUV wavelength region.

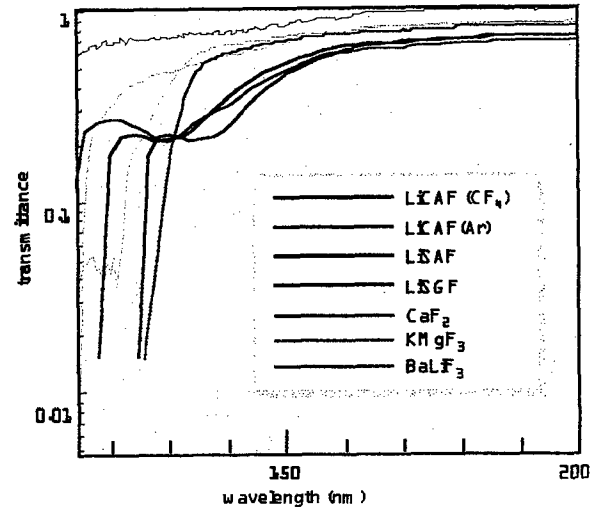


Fig.6 Transmission spectra of different fluoride single crystals.

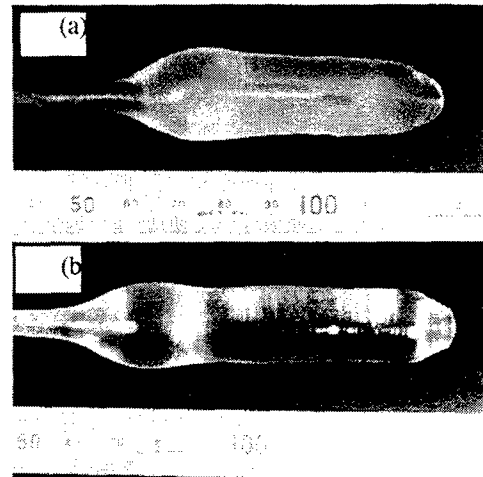


Fig.7 (a) KMgF<sub>3</sub> and (b) BaLiF<sub>3</sub> single crystals

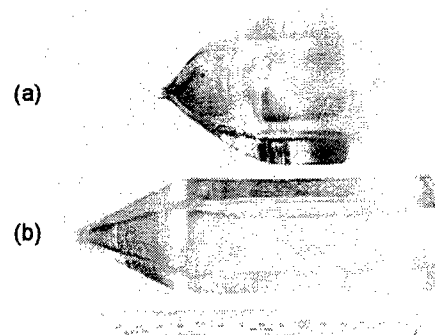


Fig.8 La<sub>3</sub>Ta<sub>0.5</sub>Ga<sub>5.5</sub>O<sub>14</sub> single crystals (a) 3-inch (b) 2-inch diameter.

### 3. NEW LANGASITE SINGLE CRYSTALS FOR PIEZOELECTRIC APPLICATIONS

The recent progress of electronic technology requires new piezoelectric crystals having properties intermediate between those of quartz and LiTaO<sub>3</sub> (LT). Currently, Langasite (La<sub>3</sub>Ga<sub>5</sub>SiO<sub>14</sub>; LGS) crystals have received attention as new candidates for piezoelectric applications<sup>13,14</sup>.

The LGS crystal has the Ca<sub>3</sub>Ga<sub>2</sub>Ge<sub>4</sub>O<sub>14</sub>-type structure with the space group P321. There are four kinds of cation sites in this structure, which can be described by the chemical formula, A<sub>3</sub>BC<sub>3</sub>D<sub>2</sub>O<sub>14</sub>. In this formula, A and B represent the decahedral (twisted Thomson cube) site coordinated by 8 oxygens, and the octahedral site coordinated by 6 oxygens, respectively. C and D represent tetrahedral sites coordinated by 4 oxygens. Different isovalent and aliovalent substitutions in a given structure are quite interesting in themselves, and could, perhaps, also result in useful structural and physical properties.

High-quality single crystals of LGS, and its aliovalent analogs La<sub>3</sub>Nb<sub>0.5</sub>Ga<sub>5.5</sub>O<sub>14</sub> (LNG) and La<sub>3</sub>Ta<sub>0.5</sub>Ga<sub>5.5</sub>O<sub>14</sub> (LTG), were grown by the conventional CZ technique<sup>15</sup>. Fig.8 shows the as-grown LTG single crystals of approximately 2 and 3 inches diameter. Pulling and rotation rates were 1mm/h and 10 rpm, respectively.

Lattice parameters of the grown crystals were found to be almost constant from shoulder to tail of the boules. Concentrations of each oxide, *i.e.* La<sub>2</sub>O<sub>3</sub>, Ga<sub>2</sub>O<sub>3</sub>, SiO<sub>2</sub>, Nb<sub>2</sub>O<sub>5</sub> and Ta<sub>2</sub>O<sub>5</sub>, were almost constant, within the estimated errors, throughout the crystallizing process. The uniformity of lattice parameter and chemical composition suggests that the stoichiometric composition is close to the congruently melting composition of the three compounds.

Synthesis of more than 70 chemical compositions were attempted. The incorporation of different A cations (Na<sup>+</sup>, Ba<sup>2+</sup>, Sr<sup>2+</sup>, Bi<sup>3+</sup>, Nd<sup>3+</sup>, etc) and B cations (Li<sup>+</sup>, Mg<sup>2+</sup>, Ga<sup>3+</sup>, Ti<sup>4+</sup>, Sb<sup>5+</sup>, Mo<sup>6+</sup>, etc) into the A and B sites was studied, respectively. Materials which showed a langasite-type single phase were crystallized in fiber form by the  $\mu$ -PD method, and subsequently their bulk crystals were also grown by the Cz technique. Bulk single crystals of Sr<sub>3</sub>Ga<sub>2</sub>Ge<sub>4</sub>O<sub>14</sub>, Na<sub>2</sub>CaGe<sub>6</sub>O<sub>14</sub>, Pr<sub>3</sub>Ga<sub>5</sub>SiO<sub>14</sub> and La<sub>3</sub>Al<sub>x</sub>Ga<sub>5-x</sub>SiO<sub>14</sub> were successfully produced by Cz technique. In Fig.9, La<sub>3-x</sub>Sr<sub>x</sub>Ta<sub>0.5+x/2</sub>Ga<sub>5.5-x/2</sub>O<sub>14</sub>, x=0.1554 (LSTG) and Sr<sub>3</sub>TaGa<sub>3</sub>Si<sub>2</sub>O<sub>14</sub> (STGS) single crystals are shown as examples.

Using LGS single crystals, we made monolithic-type filters (10.4 and 21.4 MHz) as seen in Fig.10. The electrical properties of these filters include low input and output impedance, small size and low attenuation, compared with those made of quartz (see Table I).

A 71MHz-wide passband SMD (Surface Mount Discrete-type) filter for the GSM (Global System for Mobile Communication) base station was also made, which exhibited superior properties. The main features of the electrical characteristics are listed below:

(1) Low input and output impedance (940 $\Omega$ /0.5pF, versus several k $\Omega$  for quartz filter);

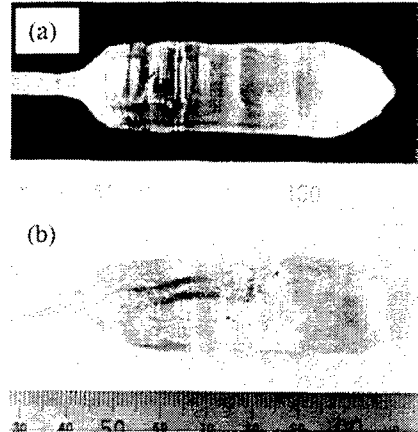


Fig.9 (a) La<sub>3-x</sub>Sr<sub>x</sub>Ta<sub>0.5+x/2</sub>Ga<sub>5.5-x/2</sub>O<sub>14</sub>, x=0.1554 and (b) Sr<sub>3</sub>TaGa<sub>3</sub>Si<sub>2</sub>O<sub>14</sub> single crystals

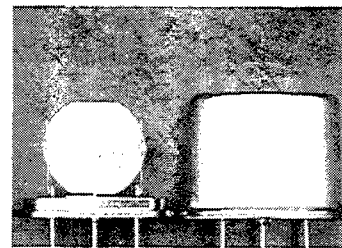


Fig.10 21.4MHz filter made of La<sub>3</sub>Ga<sub>5</sub>SiO<sub>14</sub> single crystal (size: 6.9 × 5.8 × 2.2 mm<sup>3</sup>).

Table I Electrical properties of LGS monolithic-type filters compared with quartz ones.

Frequency (MHz)	Material	Passband Width (3 dB) (kHz)	Attenuation (dB)	Input-Output Impedance (k $\Omega$ // pF)
10.7	quartz	3 ±15	2.5	5.5 k // -1.0
	LGS	3 ±15	2.0	2.5 k // 1.7
21.4	quartz	3 ±15	2.0	2.0 k // 0.5
	LGS	3 ±15	2.0	800 // 4.0
	LGS	3 ±15	2.0	1.3 k // 1.7

- (2) Interstage coupling requires only capacitors (For quartz filter, transfer is required);  
 (3) Electrode gap may be wide (approximately 100mm, vs. several mm for quartz filter).

Table II Characteristics of LNG, LTG and LGS compared with those of LT and quartz.

	LiTaO <sub>3</sub>	LGS	LNG	LTG	quartz
phase transition	exist	none	none	none	exist
melting point (°C)	1650	1490	1470	1500	—
Mohs hardness	5.5	6~7	6~7	6~7	7
electromechanical coupling factor <i>k</i> (%)	43	15~25	~30	~30	7
Q-factor	5000	30,000~ 40,000	40,000~ 60,000	40,000~ 60,000	60,000~ 80,000
equivalent series resistance (Ω)	—	5~10	2~5	2~5	10~20
thermal stability (ppm) (-20~70°C)	200~400	~150	~150	~150	10~20

In Table II, the characteristics of LNG, LTG and LGS are given, along with those of LT and quartz. Since LNG, LTG and LGS have no phase transitions and have lower melting point and higher hardness, the possibility of growing high-quality crystals allowing easy processing is expected to be likely. Their electromechanical coupling factors *k* and thermal frequency stability are between those of LT and quartz. The above characteristics indicate that LGS-family crystals are more promising materials for piezoelectric devices than lithium tetraborate (Li<sub>2</sub>B<sub>4</sub>O<sub>7</sub>) and berlinite single crystals, which have similar piezoelectric properties<sup>14</sup>.

Li<sub>2</sub>B<sub>4</sub>O<sub>7</sub> is easily soluble in all acids and bases, and easily deliquescent in air, while berlinite single crystals are difficult to grow to a large size.

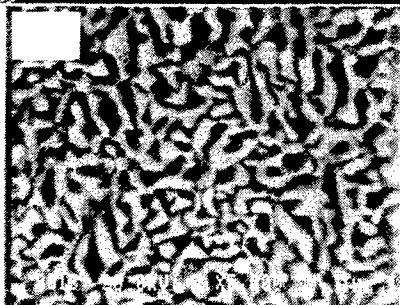
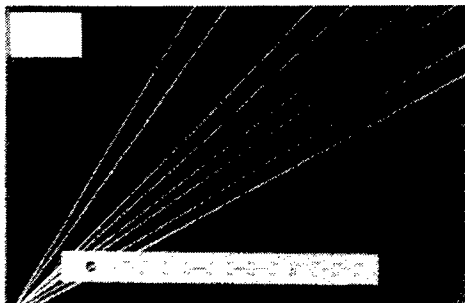


Fig.12 (a) Eutectic fibers and (b) back scattered electron image of Al<sub>2</sub>O<sub>3</sub>/Y<sub>3</sub>Al<sub>5</sub>O<sub>12</sub> fibers.

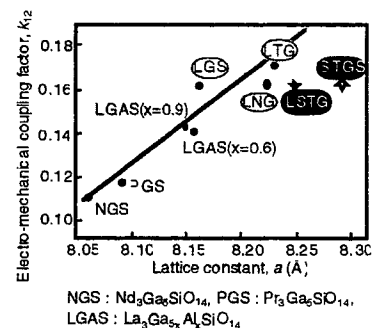


Fig.11 Electro-mechanical coupling factor vs. lattice constant.

Fig.11 shows the dependence of the electro-mechanical coupling factor, *k*<sub>12</sub>, on the lattice parameter *a* in the langasite-type crystals. As can be seen from the figure, an increase in lattice parameter *a* leads to an increase of the electro-mechanical coupling factor, *k*<sub>12</sub>. The electro-mechanical coupling factor of LTG is the largest of the langasite-type crystals studied. Therefore, we conclude that substitution of the B site is effective for improvement of the piezoelectric properties. This tendency serves as a guide for development of improved compounds of langasite-type structure.

#### 4. FIBER CRYSTALS

Directionally solidified ceramic eutectics are drawing a strong interest because of their high structural stability up to the melting temperature. Recently, promising results were reported for Al<sub>2</sub>O<sub>3</sub>/Y<sub>3</sub>Al<sub>5</sub>O<sub>12</sub> (YAG)<sup>16-18</sup> and Al<sub>2</sub>O<sub>3</sub>/GdAlO<sub>3</sub><sup>19</sup> systems. However, because of processing difficulties, the experimental data for oxide eutectics are still limited and often uncertain.

We have applied the  $\mu$ -PD method for the growth of Al<sub>2</sub>O<sub>3</sub>/YAG

eutectic fibers. The  $\mu$ -PD method involves downward pulling of a crystalline fiber 0.1-2.0 mm in diameter through a capillary hole arranged in a crucible bottom. The  $\mu$ -PD features two points important for eutectic growth: (1) a very high axial temperature gradient exists near the growth interface of the order of  $3-5 \times 10^3 \text{ }^\circ\text{C/cm}^{20}$ . It permits high pulling rates and assures a planar interface and process stability. Secondly, (ii) composition is always uniform along the fiber length, since melt convection is impossible inside the narrow capillary channel.

A high-temperature version of  $\mu$ -PD employed an iridium crucible directly coupled to the RF power generator. A sapphire <0001> seed was used for growth of the eutectic fibers. The starting materials were 4N purity  $\text{Al}_2\text{O}_3$  and  $\text{Y}_2\text{O}_3$  in the molar ratio of 81.3 mol %  $\text{Al}_2\text{O}_3$  to 18.7 mol %  $\text{Y}_2\text{O}_3$ <sup>21</sup>.

Eutectic fibers 0.25-1.00 mm in diameter and up to 500 mm in length were grown over a range of pulling rate 0.15 - 10.00 mm/min (see Fig.12). Samples of eutectic fibers grown under various pulling rates were examined using scanning electron microscopy (SEM). Several fibers were grown at a step-variable pulling rate starting from 0.15 and up to 10 mm/min. In all these experiments, the 'Chinese script' type structure was found to possess excellent reproducibility, whereas the cellular structure was not found at all. (The microstructure of eutectic sometimes forms the structure, which is resembles to Chinese character. Such microstructure is called 'Chinese-script type' microstructure.) The volume fraction of YAG was  $0.45 \pm 0.02$  for all types of structure including inter-cell areas, which corresponds exactly to the theoretical value for the eutectic composition (0.44). The characteristic script size was found to be very uniform for each cross-section studied. Experimentally, the generally accepted relation  $\lambda \sim v_p^{-1/2}$ , where  $\lambda$  is interlamellar spacing of a conventional lamellar structure and  $v_p$  is the solidification rate, also applies to the script structure of the  $\text{Al}_2\text{O}_3/\text{YAG}$  system. The constant of proportionality was found to be 10, if  $\lambda$  has dimensions of mm and  $v_p$  mm per second. This value is large enough to allow effective microstructure control by changing solidification rate

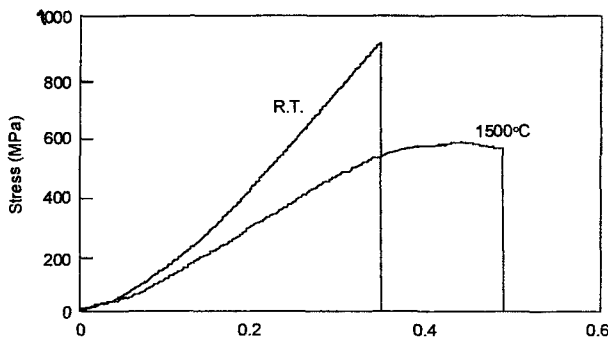


Fig.13 Tensile stress-displacement curves of  $\text{Al}_2\text{O}_3/\text{Y}_3\text{Al}_5\text{O}_{12}$  eutectic fibers (grown in Ar gas atmosphere).

The composite has been shown to have high mechanical strength up to 1800  $^\circ\text{C}$ , excellent oxidation resistance, high thermal stability of microstructure and thermal shock stability (Fig.13).  $\text{Al}_2\text{O}_3/\text{Y}_3\text{Al}_5\text{O}_{12}$  showed a tensile strength of 620 MPa at 1500  $^\circ\text{C}$  in vacuum. This is the highest strength at this temperature to date.

### 5. $\beta$ - $\text{Ga}_2\text{O}_3$ AS TRANSPARENT CONDUCTIVE OXIDE

$\beta$ - $\text{Ga}_2\text{O}_3$  is transparent with a band gap of 4.8 eV, and belongs to the space group C2/m. It is intrinsically an insulator, but its n-type semiconduction when grown under reducing conditions is well known<sup>22</sup>. An undesired side effect is the resulting blue coloration, and thus degradation of the transmission, a fundamental property for window applications such as displays, solar cells, etc. Improvement of electrical conductivity through the addition of dopants while preserving the transparency of the pure  $\beta$ - $\text{Ga}_2\text{O}_3$  makes of this material a substitutive candidate for transparent conductive oxides (TCOs). Moreover, its shorter absorption edge will allow to extend the application fields of TCOs.

Powders of  $\text{Ga}_2\text{O}_3$ ,  $\text{WO}_3$  and  $\text{HfO}_2$  of nominal 4N purity were mixed, sintered and grown to single crystals using the floating zone (FZ) technique with a double ellipsoid image furnace (ASGAL Co.:SS-10W). The growth was done under previously optimized conditions: growth rate of 5 mm/h, simultaneous rotation of feed and seed rods at 20 rpm in opposite directions, 500 ml/min. gas flow of different  $\text{N}_2/\text{O}_2$  mixtures. The grown crystals had typical length of 3-4 cm, and diameter varying between 0.5 and 1 cm. For transmission and electrical measurements, crystals were cleaved in the (001) plane to obtain thin platelet-like samples, which exhibited flat, reflective surfaces.

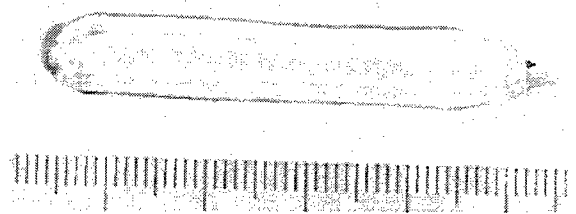


Fig.14. Nominally pure  $\beta$ - $\text{Ga}_2\text{O}_3$  single crystal grown under pure  $\text{O}_2$  and a pressure of 2 atmosphere.

The optical and electrical properties of the as-grown crystals depended on the concentration of the dopants and on the

oxygen partial pressure. Crystal growth from nominally undoped feed rods under 1 atmosphere pressure was impossible due to the appearance and explosion of bubbles, which destabilized the molten zone. The formation of bubbles could be suppressed by the increase of pressure to 2 atmospheres (Fig.14), or by the incorporation of W or Hf as dopants. Fig.15 and Fig.16 show the crystals grown under pure O<sub>2</sub> and 1 atmosphere pressure, with a nominal composition of the feed rod of 6 mol.% WO<sub>3</sub> and 0.2 mol.% HfO<sub>2</sub>, respectively. These crystals were visually homogeneous, transparent, colorless and without cracks or inclusions. Improved transmittance and conductivity could be also achieved, indicating the beneficial effects of the substitution of Ga<sup>3+</sup> by W<sup>4+</sup> or Hf<sup>4+</sup> and the potential optimization of Ga<sub>2</sub>O<sub>3</sub> properties for TCO applications.

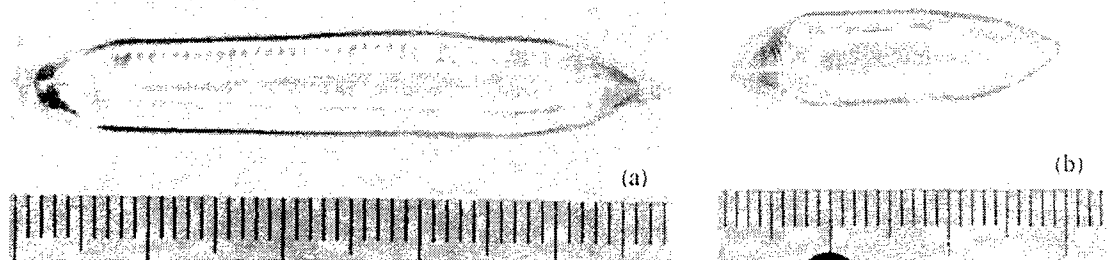


Fig. 15 (a) W-doped and (b) Hf-doped  $\beta$ -Ga<sub>2</sub>O<sub>3</sub> single crystals grown under pure O<sub>2</sub>, 1atm pressure.

## 6. CONCLUSIONS

Various new fluoride and oxide crystals were developed. Ce:LiCAF and Ce:LiSAF single crystals of 18 mm diameter were grown by the CZ technique under CF<sub>4</sub> atmosphere. Under the same growth conditions, Ce:LiCAF single crystals of 50 mm diameter (2 inch) were also grown up to a solidification fraction of 60 %. Laser output energy of 60 mJ was obtained. This demonstrates that Ce:LiCAF is a promising material for high-energy UV pulse generation. KMF and BLF single crystals of 20 mm diameter were also grown. LiCAF, LiSAF, KMF and BLF single crystals showed a transmission edge at 112 nm, 119 nm, 115 nm and 120 nm, respectively. These characteristics indicate the high potential of these crystals as optical materials. A series of new promising langasite-type materials were found. LGS, LNG and LTG single crystals with maximum size of 3 inches in diameter were successfully grown by the Czochralski technique. Prototype models of wide passband filters were prepared using these crystals. LGS, LNG and LTG single crystals showed to have superior piezoelectric properties compared to other compounds with properties intermediate between those of quartz and LT. By applying the high-temperature  $\mu$ -PD technique, directionally-solidified eutectic Al<sub>2</sub>O<sub>3</sub>/REAG fibers were grown. Al<sub>2</sub>O<sub>3</sub>/Tm<sub>3</sub>Al<sub>5</sub>O<sub>12</sub> showed a tensile strength of 620 MPa at 1500 °C in vacuum. Undoped and doped  $\beta$ -Ga<sub>2</sub>O<sub>3</sub> single crystals were grown by the FZ technique. The substitution of Ga<sup>3+</sup> by W<sup>4+</sup> or Hf<sup>4+</sup> improved transmittance and conductivity, indicating the potential optimization of  $\beta$ -Ga<sub>2</sub>O<sub>3</sub> properties for TCO applications.

## ACKNOWLEDGMENT

The authors would like to acknowledge and thank to Associate Professor Dr.S.Durbin and the members of the Fukuda laboratory of the Institute for Materials Research, Tohoku University. They are also indebted to Mr.J.Sato (TDK Corporation), Mr.H.Kawanaka (Victor company of Japan, Ltd.), Mr.S.Murakami (KYOCERA Corporation) for their many contributions.

## REFERENCES

1. N.Sarukura, M.A.Dubinskii, Z.Liu, V.V.Semashko, A.K.Naumov, S.L.Korableva, R.Y.Abdulsabirov, K.Edamatsu, Y.Suzuki, T.Itoh and Y.Segawa, *IEEE J. Selected Topics in Quantum Electronics*, **1** (1995) 792.
2. M.A.Dubinskii, V.V.Semashko, A.K.Naumov, R.Y.Abdulsabirov, and S.L.Korableva, *Laser Phys.* **3** (1993) 216.
3. C.D.Marshall, S.A.Payne, J.A.Speth, W.F.Krupke, G.J.Quarles, V.Castillo and B.H.T.Chai, *J. Opt. Soc. Am.* **B.11** (1994) 2054.
4. R.F.Belt and R.Uhrin, *J. Cryst. Growth*, **109** (1991) 340.
5. K.Shimamura, N.Mujilat, K.Nakano, S.L.Baldochi, Z.Liu, H.Ohtake, N.Sarukura and T.Fukuda, *J. Cryst. Growth*, **197** (1999) 896.
6. R.D.Shannon, *Acta Cryst.* **A32** (1976) 751.



7. D.Klimm, P.Reiche, *Proceedings of International Symposium on Laser and Nonlinear Optical Materials*, 3-5 November 1997, 284.
8. Z.Liu, S.Izumida, H.Ohtake, N.Sarukura, K.Shimamura, N.Mujilatu, S.L.Baldochi and T.Fukuda, *Jpn. J. Appl. Phys.*, **37** (1998) L1318.
9. T.M.Bloomstein, M.W.Hom, M.Rothschild, R.R.Kunz, S.T.Palmacol and R.B.Goodman, *J. Vac. Sci. Technol.*, **B 15** (1997) 2112.
10. Al.Darabont, C.Neamtu, S.I.Farcas and Gh.Borodi, *J. Cryst. Growth*, **169** (1996) 89.
11. R.C.DeVries and R.Roy, *J. Am. Chem. Soc.*, **75** (1953) 2481.
12. S.L.Baldochi, K.Shimamura, K.Nakano, N.Mujilatu and T.Fukuda, *J. Cryst. Growth*, **200** (1999) 521.
13. I.M.Silvestrova, Yu.V.Pisarevsky, V.V.Bezdelkin, P.A.Senyushenkov, *Proc. 1993 IEEE International Frequency Control Symposium*, p.351.
14. J.Detaint, J.Schwartzel, A.Zarka, B.Capelle, J.P.Denis, E.philippot, *Proc. 1994 IEEE International Frequency Control Symposium*, p.58.
15. K.Shimamura, H.Takeda, T.Kohno and T.Fukuda, *J. Cryst. Growth*, **163** (1996) 388.
16. T.A.Parthasarathy, T.I.Mah, L.E.Matson, *J. Am. Ceram. Sci.*, **76** (1993) 29.
17. Y.Waku, N.Nakagawa, H.Ohtsubo, Y.Ohsora, Y.Kohtoku, *J. Jpn. Inst. Metals*, **59** (1995) 71.
18. Y.Waku, H.Ohtsubo, N.Nakagawa, Y.Kohtoku, *J. Mater. Sci.*, **31** (1996) 4663.
19. Y.Waku, N.Nakagawa, T.Wakamoto, H.Ohtsubo, K.Shimizu, Y.Kohtoku, *Nature*, **389** (1997) 49.
20. S.Uda, J.Kon, J.Ichikawa, K.Inaba, K.Shimamura, T.Fukuda, *J. Cryst. Growth*, **179** (1997) 567.
21. D.Viechnicki, F.Schmid, *J. Mater. Sci.*, **4** (1969) 84.
22. N.Ueda, H.Hosono, R.Waseda and H.Kawazoe, *Appl. Phys. Lett.*, **70** (1997) 3591.